pH-Dependent production of molecular chlorine, bromine, and iodine from frozen saline surfaces

John W. Halfacre[1], Paul B. Shepson[2,3,4], Kerri A. Pratt[5]

[1]Department of Chemistry, Indiana University Southeast, New Albany, IN USA
[2]Department of Chemistry, Purdue University, West Lafayette, IN USA
[3]Department of Earth, Atmospheric, and Planetary Sciences, Purdue University, West Lafayette, IN USA
[4]School of Marine and Atmospheric Sciences, Stony Brook University
[5]Department of Chemistry and Earth & Environmental Sciences, University of Michigan, Ann Arbor, MI USA

Correspondence to: J. W. Halfacre (halfacre@ius.edu)

Abstract

The mechanisms of molecular halogen production from frozen saline surfaces remain incompletely understood, limiting our ability to predict atmospheric oxidation and composition in polar regions. In this laboratory study, condensed-phase hydroxyl radicals (OH) were photochemically generated in frozen saltwater solutions that mimicked the ionic composition of ocean water. These hydroxyl radicals were found to oxidize Cl^-, Br^-, and I^-, leading to the release of Cl_2, Br_2, I_2 and IBr. At moderately acidic pH (buffered between 4.5-4.8), irradiation of ice containing OH-precursors (either of hydrogen peroxide or nitrite ion) produced elevated amounts of I_2. Subsequent addition of O_3 produced additional I_2, as well as small amounts of Br_2. At lower pH (1.7-2.2) and in the presence of an OH precursor, rapid dark conversion of I^- to I_2 occurred from reactions with hydrogen peroxide or nitrite, followed by substantial photochemical production of Br_2 upon irradiation. Exposure to O_3 under these low pH conditions also increased production of Br_2 and I_2; this likely results from direct O_3 reactions with halides, as well as the production of gas-phase HOBr and HOI that subsequently diffuse to frozen solution to react with Br^- and I^-. Photochemical production of Cl_2 was only observed when the irradiated sample was composed of high-purity NaCl and hydrogen peroxide (acting as the OH precursor) at pH =1.8. Though condensed-phase OH was shown to produce Cl_2 in this study, kinetics calculations suggest that heterogeneous recycling chemistry may be equally or more important for Cl_2 production in the Arctic atmosphere. The condensed-phase OH-mediated halogen production mechanisms demonstrated here are consistent with those proposed from recent Arctic field observations of molecular halogen production from snowpacks. These reactions, even if slow, may be important for providing seed halogens to the Arctic atmosphere. Our results suggest the observed molecular halogen products are dependent on the relative concentrations of halides at the ice surface, as we only observe what diffuses to the air-surface interface.

48 1 **Introduction**

49   It is now well-established that gas-phase halogen species influence atmospheric composition through reactions

50 with ozone (O_3), volatile organic compounds (VOCs), and gaseous elemental mercury (Hg^0) (Barrie and Platt, 1997;

51 Carpenter et al., 2013; Platt and Hönninger, 2003; Saiz-Lopez and von Glasow, 2012; Simpson et al., 2007, 2015;

52 Steffen et al., 2008, 2014, and references therein). In polar regions, it is believed that halogens build up to effective

53 concentrations through a heterogeneous reaction sequence known as the "halogen explosion" (Reactions R1-4, where

54 X represents Cl, Br, or I) (Garland and Curtis, 1981; Tang and McConnell, 1996; Vogt et al., 1996; Wennberg, 1999).

55 $X_2 + h\nu \rightarrow 2X$ (R1)

56 $X + O_3 \rightarrow XO + O_2$ (R2)

57 $XO + HO_2 \rightarrow HOX + O_2$ (R3)

58 $HOX + X^- + H^+ \rightarrow X_2 + H_2O$ (R4)
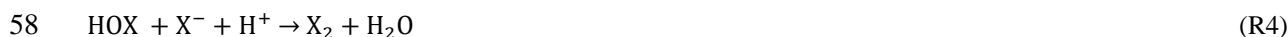
59 In this sequence, a molecular halogen (X_2) is photolyzed to produce two reactive halogen radicals. These radicals can

60 react with O_3 to produce halogen oxides (XO). The XO produced in Reaction R2 rapidly photolyzes (or reacts with

61 NO) to regenerate O_3 and X_2 in a null cycle. To irreversibly remove ambient O_3, XO must react with another halogen

62 oxide or Hg^o. Alternatively, XO can react with HO_2 to form HOX (Reaction R3) or NO_2 to form $XONO_2$. Gas-phase

63 HOX can heterogeneously react with salt-laden surfaces, including sea-salt aerosol particles (McConnell et al., 1992)

64 and the "disordered interface" (often referred to as a quasi-liquid or quasi-brine layer) that exists on frozen saline

65 surfaces (Bartels-Rausch et al., 2014; Cho et al., 2002) to produce X_2, effectively returning two halogen radicals to

66 the gas phase. Additionally, this mechanism is enhanced under acidic conditions, confirmed by laboratory studies of

67 aqueous (Fickert et al., 1999) and frozen solutions (e.g., Abbatt et al., 2010; Sjostedt and Abbatt, 2008; Wren et al.,

68 2013), and from field observations (Pratt et al., 2013).

69   While much has been learned about the atmospheric chemistry of reactive halogen species in the Arctic,

70 knowledge gaps remain in the chemical mechanisms by which molecular halogens are produced from frozen surfaces

71 (Liao et al., 2014; Pratt et al., 2013). Recently, in situ, light-induced production of Cl_2 (Custard et al., 2016), Br_2 (Pratt

72 et al., 2013; Raso et al., 2017), and I_2 (Raso et al., 2017) within snowpack interstitial air has been reported, and was

73 further demonstrated to be enhanced following the addition of O_3. The Br_2-producing snowpacks studied by Pratt et

74 al. (2013) were characterized as having larger surface area, lower pH (≤ 6.3), greater [Br^-]/[Cl^-] molar ratios ($\geq 1/148$),

75 and lower salinity relative to other frozen samples collected near Utqiaġvik, Alaska. The proposed mechanism for this

76 chemistry is based on laboratory studies of condensed-phase, hydroxyl radical (OH)-mediated halogen oxidation

77 (Reactions R5-R12), that is followed by partitioning of the molecular halogen to the gas phase (Abbatt et al., 2010;

78 Knipping et al., 2000; Oum et al., 1998b).

79 $H_2O_2 + h\nu \rightarrow 2\ OH$ (R5)

80 $NO_2^- + h\nu \rightarrow NO + O^-$ (R6)

81 $O^- + H^+ \rightarrow OH$ (R7)

82 $OH + X^- \leftrightarrow HOX^-$ (R8)

83 $HOX^- + H^+ \rightarrow X + H_2O$ (R9)

84 $X + X^- \leftrightarrow X_2^-$ (R10)

85 $2X_2^- \rightarrow X_3^- + X^-$ (R11)

86 $X_3^- \leftrightarrow X^- + X_2$ (R12)
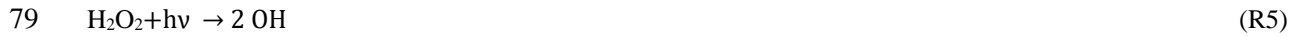
87 Direct, light-induced halogen production from frozen surfaces in the presence of OH has been previously demonstrated

88 in the laboratory for Br_2 and possibly for I_2 (Abbatt et al., 2010), but analogous chemistry for Cl_2 has yet to be observed.

89 Additionally, photochemical production of I_2 has been directly observed in the absence of OH (Kim et al., 2016).

90 Employing cavity ring-down spectroscopy, Kim et al. (2016) reported photochemical production of I_2 from a frozen

91 solution by known aqueous-phase chemistry (R13-17). This proposed photochemical mechanism involves an (I^--O_2)

92 charge-transfer complex (Levanon and Navon, 1969).

93 $O_2(aq) + 4H^+ + 6I^- \rightarrow 2I_3^- + 2H_2O$ (R13)

94 $I^- + O_2 \rightarrow (I^-O_2) \xrightarrow{h\nu} I + O_2^-$ (R14)

95 $I + I^- \leftrightarrow I_2^-$ (R15)

96 $2I_2^- \rightarrow I_3^- + I^-$ (R16)

97 $I_3^- \leftrightarrow I^- + I_2$ (R17)

98 Kim et al. (2016) also report enhanced photochemical I_3^- production (determined spectrophotometrically) from sunlit

99 frozen iodide solutions placed on Antarctic snowpack, as well as from refrozen field snow and glacier samples doped

100   with iodide. A question is thus raised regarding the necessity of OH for I_2 production under environmentally-relevant

101   conditions.

102   The role of O_3 in halogen production on frozen surfaces is also unclear. Previous laboratory studies have

103   demonstrated that halide-doped frozen surfaces exposed to O_3 can lead to Br_2 production (independent of radiation,

104   R18-R19, and R4) (Oldridge and Abbatt, 2011; Oum et al., 1998a; Wren et al., 2013).

105     $O_3 + Br^- \leftrightarrow BrO^- + O_2$ (R18)

106     $BrO^- + H^+ \leftrightarrow HOBr$ (R19)

107   It has recently been shown that this process proceeds at the surface, through a water-stabilized ozonide, $Br \cdot OOO^-$, as

108   shown in reactions R20-R22.   Artiglia et al. (2017) observed this $Br \cdot OOO^-$ intermediate via liquid-injection X-ray

109   photoelectron spectroscopy.

110     $Br^- \;+\;\; O_3 \;\;\;\;\;\; \rightarrow \;\;\;\;\;\; Br \cdot OOO^-$ (R20)

111     $Br \cdot OOO^- \;+\; H^+ \rightarrow \;\;\;\;\;\; HOBr \;+\; O_2$ (R21)

112     $Br \cdot OOO^- \;+\; H_2O \;\;\rightarrow \;\;\; HOBr \;+\; O_2 \;+\; OH^-$ (R22)

113   Wren et al. (2013) found that Cl_2 was produced primarily via heterogeneous recycling of HOCl, resulting from BrCl

114   photolysis, on halide-rich artificial snow. However, the observation that O_3 induces halogen production from natural

115   frozen surfaces has yet to be confirmed by field observations of snowpack chemistry, in which exposure to only O_3 in

116   the absence of light has not been shown to produce molecular halogens (Custard et al., 2017; Pratt et al., 2013; Raso

117   et al., 2017). This raises a question of whether O_3 is more important for initial halogen release, or in a gas phase

118   propagation/recycling capacity (i.e., per the halogen explosion).

119   In this study, we utilized a custom ice-coated-wall flow reactor in tandem with chemical ionization mass

120   spectrometry (CIMS) to study Br_2, Cl_2, and I_2 production from frozen surfaces with compositions mimicking sea ice.

121   The effects of photochemically generated OH radicals, O_3 addition, and pH are tested as they relate to the production

122   of these halogens. Surface pH was controlled through use of buffers.

123 **2** **Methods**

124 **2.1** **Materials**

125   Sample solutions were composed to mimic the halide composition of seawater. This was achieved using

126 either dissolved Instant Ocean (Spectrum Brands), or commercially available halide salts at a composition that mimics

127 Instant Ocean (for consistency) in solutions referred to hereafter as "saltwater." The halide concentrations in these

128 solutions were made to a final concentration of 0.56M Cl^-, 7.2 x 10^{-4} M Br^-, and 1.9 x 10^{-6} M I^-. Except for Instant

129 Ocean, all chemicals were purchased from Sigma Aldrich. Halide salts include solid NaCl (puriss. p.a. grade, ≥99.5%

130 purity), NaBr (puriss. grade, >99% purity), KI (puriss. p.a. grade, ≥99.5% purity). We note that these halide

131 concentrations are comparable to those in actual seawater (Herring and Liss, 1974; Luther et al., 1988; Tsunogai and

132 Sase, 1969), which typically contains Cl^-, Br^-, and I^- at ratios of 1:$^1/_{660}$:$^1/_{200,000}$. Solutes were dissolved in ultrapure

133 water (Birck Nanotechnology Center). Dissolved organic carbon for Instant Ocean and halide salt solutions were

134 analyzed using a Shimadzu TOC-V$_{CSH}$ Total Organic Carbon Analyzer, and determined at approximately 70 mg/L for

135 Instant Ocean solutions, and less than 5 mg/L for saltwater solutions. No further characterization of carbon-containing

136 compounds was performed.

137   While previous investigators have adjusted the pre-freezing pH of their samples, it is very difficult to know

138 the pH in the surface brine (or disordered interface) of frozen samples (Bartels-Rausch et al., 2014), though there is

139 evidence from laboratory studies suggesting that the pH of salt solutions remains largely unchanged after freezing

140 (Wren and Donaldson, 2012b). To obviate this problem, the aqueous solutions used in this study were buffered so

141 that the same pH should exist in the surface brine layer. All solutions were buffered by either a 20 mM acetic acid

142 (ACS reagent grade, ≥99.7% purity)/acetate (puriss. p.a. grade) buffer (pH ≈ 4.5-4.7), or a 20 mM bisulfate

143 (ReagentPlus grade, 99% purity)/sulfate (ReagentPlus grade, ≥ 99.0% purity) buffer (pH ≈1.7 – 2.2). These buffer

144 concentrations were chosen as a compromise between using as little buffer as possible, yet enough buffer to ensure

145 adequate buffering ability, as buffer capacity rapidly decreases as constituent species concentrations approach the acid

146 K_a value. pH values of sample solutions were determined before and after experiments with no significant changes

147 observed, suggesting the buffer composition/buffering capacity does not appreciably change over the course of an

148 experiment (discussed further in the Supplemental Information). 100 μM of either hydrogen peroxide (trace analysis

149   grade, $\geq$ 30% purity) or sodium nitrite (ReagentPlus grade, $\geq$ 99.0% purity) were included as photochemical hydroxyl

150   radical precursors, via reactions R5, and R6-7.

2.2   Flow tube

152   Experiments were performed in a custom-built 150 cm long, 2.5 cm ID frozen-walled Pyrex flow tube

153   contained within a temperature-controlled cooling jacket. In each experiment, 80.0 mL of sample solution was poured

154   into the tube in the presence of room air, which was subsequently sealed with vinyl caps (McMaster-Carr). The flow

155   tube was then rotated on motorized rollers within a 170 cm x 50 cm x 50 cm, insulated wooden cooling chamber.

156   Crushed dry ice was placed along the bottom of the chamber, and fans were used to circulate the air throughout the

157   chamber such that the flow tube was evenly cooled. After ~30 minutes, the sample was evenly frozen (ice thickness

158   of 0.9 mm). The flow tube was subsequently transferred to an enclosed 156 cm x 50 cm x 50 cm wooden, Mylar-

159   lined experiment chamber, and connected to a recycling chiller set to 258 K (i.e., above the NaCl•$2H_2O$ eutectic point,

160   in which the relevant chemical reactions are expected to occur with / in a brine on the ice surface (Cho et al., 2002;

161   Oldridge and Abbatt, 2011)). This conjecture is based on the work of Oldridge and Abbatt (2011), who reported from

162   a series of similar experiments that when O_3 is flowed over frozen NaCl/NaBr solutions above the NaCl eutectic

163   temperature, reaction kinetics were strongly consistent with chemistry occurring in a liquid brine. The cooling liquid

164   used for the chiller was a mixture of 60% ethylene glycol and 40% distilled water. Six UVA-340 solar simulator

165   lamps (Q-Lab, 295 – 400 nm with maximum wattage at 340 nm, irradiance spectrum in Fig. S1) were installed in the

166   experiment box (two on each side except bottom). Each side was lined with reflective Mylar sheets to evenly irradiate

167   the flow tube when the lamps were powered.

168   A flow schematic representing typical experiments is shown in Fig. 1. The carrier gas (Air, Ultra Zero grade,

169   Praxair) was scrubbed of volatile organic compounds using activated charcoal, and water by travelling through coiled

170   stainless-steel tubing surrounded by crushed dry ice (replaced throughout the course of an experiment). This gas was

171   measured to contain $\leq$ 300 – 400 pmol mol^{-1} NO (experimentally determined limits of detection) using the Total

172   REactive Nitrogen Instrument (TRENI) (Lockwood et al., 2010; Xiong et al., 2015). Though NO_2 was not measured,

173   it should have been removed by the charcoal trap. Before entering the coated-wall flow tube, the carrier gas flowed

174   through a commercial O_3 generator (2B Technologies model 306). Carrier gas air entered the tube near room

175   temperature (20 °C). At the start of experiments, the O_3 generator was set to 0 nmol mol^{-1}. Carrier gas then entered

176   the flow tube in the dark experiment chamber. In most experiments, the carrier gas was regulated to a volumetric flow

177   rate of 4.0 L min^{-1}, which yields a residence time in the flowtube of ~12 seconds. On exiting the flow tube, sample

178   air was characterized using a Thermo Environmental 49i O$_3$ monitor (flow rate of ~1.5 L min^{-1}) and a chemical

179   ionization mass spectrometer (CIMS, sampling flow rate of ~1.7 L min^{-1}, described below in Sect 2.3). Excess flow

180   air was vented away. At set times in an experiment, the solar simulator bulbs were activated, and O$_3$ was added to the

181   system by powering the O$_3$ generator. At the end of each experiment, the ice was melted and the water collected for

182   pH measurements. To clean the flow tube, its interior was washed three times with ultrapure water before a final rinse

183   with wash acetone. The flow tube was then connected to a compressed nitrogen gas cylinder (Praxiar, >99.99% purity)

184   to dry for at least 2 hours. Once dry, the flow tube was disconnected and capped until the next experiment.

185   **2.3   CIMS**

186   Halogen species were detected using a chemical ionization mass spectrometer (CIMS), described previously

187   by Liao et al. (2011) and Pratt et al. (2013). Chemical ionization is achieved by ion-molecule reactions that occur

188   between iodide-water reagent clusters, I(H$_2$O)$_n^-$ in N$_2$, and the gas-phase analytes in zero air. The iodide-water clusters

189   are formed when gas-phase iodide ions, generated by flowing 5 ppm methyl iodide through a ^{210}Po ionizer (NRD)

190   combines with water in the humidified ion-molecule region of the CIMS. Ion were filtered using a quadrupole mass

191   filter. The ice-coated flowtube was connected to the CIMS via approximately 50 cm of i.d. 1/2″ PFA Teflon tubing.

192   A typical CIMS sampling cycle consisted of an 8.35s duty cycle. Dwell times for all monitored species were

193   250 ms except for the reagent ion (detected as m/z 147, I(H$_2$^{18}O)$^-$), which was set to a dwell time of 100 ms. The 18

194   ions analyzed in this study are listed in Table 1, but we focus herein on results concerning masses related to Br$_2$ (m/z

195   285 and 287: I^{79}Br^{79}Br$^-$ and I^{81}Br^{79}Br$^-$, respectively), Cl$_2$ (m/z 197, 199, and 201: I^{35}Cl^{35}Cl$^-$, I^{37}Cl^{35}Cl$^-$, and I^{37}Cl^{37}Cl$^-$),

196   and I$_2$ (m/z 381: I$_3^-$). In addition, IBr (m/z 333 and 335: I^{79}IBr$^-$, I^{81}IBr$^-$) was unambiguously detected in some

197   experiments. The presence of Br$_2$, Cl$_2$, and IBr was confirmed by measuring the ratios between the two isotope signals

198   for each mass, compared to the natural abundances (i.e., 1.95 for m/z 287:285; 1.54 for m/z 197:199; and 1.03 for m/z

199   333:335, respectively). Data outside ±25% the expected isotope ratio were excluded from analysis. The signals for

200   BrCl (m/z 241 and 243: I^{79}Br^{35}Cl$^-$, I^{81}Br^{35}Cl$^-$, I^{79}Br^{37}Cl$^-$) masses were never observed at the correct ratios (1.3 for m/z

201   243:241), and so those data were not reported here. As the introduction of ~60 nmol mol^{-1} O$_3$ to the experimental

202   system significantly increased the baseline signal of m/z 197, but not m/z 199 or 201, the presence of Cl$_2$ could not be

203 confirmed under elevated O_3 conditions. In addition, background subtracted, relative signals for m/z 271 (IHOI$^-$) and

204 m/z 225 (IHO^{81}Br$^-$) are discussed (signals are relative to that of the ionization gas (m/z 147, I(H$_2$^{18}O)$^-$)). According to

205 isotope ratios, IHOBr$^-$ was not unambiguously observed, however, due to an interference at m/z 223 (IHO^{79}Br$^-$), and

206 our results here should be considered for only qualitative purposes as we only discuss relative changes in the signal.

207 CIMS calibrations were performed using I_2, Br_2, and Cl_2 permeation devices (VICI) at the start and

208 conclusion of each experiment. Br_2 and Cl_2 permeation outputs were quantified using the spectrophotometric method

209 described by Liao et al. (2012). The I_2 permeation output was quantified by flowing the I_2 through an impinger

210 containing a NaHCO$_3$ (30mM)/NaHSO$_3$ (5mM) reducing solution. This solution quantitatively reduces I_2 to I$^-$, which

211 was then determined using a Dionex DX500 ion chromatography system. Permeation rates were calculated for each

212 experiment and found to average $(1.9\pm0.1) \times 10^{-11}$, $(5.5\pm0.1) \times 10^{-10}$, and $(8.6\pm0.1) \times 10^{-10}$ mol min^{-1} of I_2, Br_2, and

213 Cl_2, respectively (uncertainties representing standard error of the mean). CIMS calibration factors were calculated for

214 individual experiments. These factors are based on the average of the signal sensitivities, determined from the

215 permeation sources, calculated at the start and completion of each experiment. Corresponding uncertainties for these

216 calibration factors thus represent the 1σ standard deviation of the mean sensitivity. An approximate I^{79}IBr$^-$ calibration

217 factor was assumed to be the average of the sensitivities for m/z 287 (IBr$_2$$^-$) and 381 (I$_3$$^-$). Background measurements

218 were performed before and after the experiment (minimum of 5 min) by passing the carrier gas through the

219 experimental flow tube (without O_3, in the dark), and subsequently through a glass wool scrubber, previously shown

220 to remove molecular halogens with greater than 95% efficiency (Liao et al., 2012; Neuman et al., 2010). Temporal

221 variations in bromine-species signals while using the low pH sulfate/bisulfate buffer were observed in some

222 experiments (Fig. S2) and are discussed in the Supplementary Information.

223 Analysis of experimental data was based on one-minute averages, with uncertainties representing the

224 standard deviation of these averages. Subsequently, signals were converted to concentrations using the sensitivities

225 calculated above, propagating the sensitivity uncertainty into the measurement uncertainty. Average limits of

226 detection (3σ) across all experiments for the molecular halogens during background periods were 1.8 ± 0.4, 1.2 ± 0.3,

227 and 9 ± 2 pmol mol^{-1} for Br_2, Cl_2, and I_2 respectively (uncertainties representing standard error of the mean).

228 Additionally, reported uncertainties for integrated amounts of formed halogens are calculated as integrated halogen

229 concentrations multiplied by the relative uncertainty in the CIMS signal sensitivity.

3   Results and Discussion

The experiments described here address the extent to which condensed-phase OH radicals in an ice surface brine (Cho et al., 2002) can produce I_2, Br_2, and Cl_2 through condensed-phase reactions within frozen saline surfaces, as hypothesized by recent field (Custard et al., 2017; Pratt et al., 2013; Raso et al., 2017) and laboratory experiments (Abbatt et al., 2010). In addition, we test the pH-dependence of this chemistry and whether gas-phase O_3 enhances this production. We find the relative and absolute amounts of halogens produced from ice are a complex function of the relative concentrations of the precursor halide ions, pH, presence of oxidants, radiation, and O_3.

The ice-coated flow tube experiments started under dark conditions and without addition of O_3 (Sect. 3.1). Once signals stabilized, lights were activated (Sect. 3.2). After 1-2 hours, ~60 nmol mol^{-1} of O_3 was introduced into the carrier gas (Sect. 3.3). Integrated amounts of produced molecular halogens are presented in Table 2 for all experiments. Unless otherwise specified, integrated amounts of produced halogens represent amounts produced over the course of 1 h of exposure to light (Sect. 3.2) and/or ozone (Sect. 3.3). Saline ices tested include frozen Instant Ocean (IO) solutions, "saltwater" (SW) solutions composed of dissolved reagent grade salts mimicking seawater composition, and 0.56 M high purity NaCl (CL1). OH-radical precursors used include hydrogen peroxide (H_2O_2) or nitrite (NO_2^-), which have been estimated to account for 96% of snowpack photochemical OH formation at Utqiaġvik, AK (France et al., 2012). Many of the salient features of our results are demonstrated by example experiments shown in Fig. 2, including the impact of irradiation in the presence of ice phase OH radical precursors, varied pH, and the presence of O_3. Below we discuss the results and interpretations of our experiments, organized by the mechanism of halogen production and halogen products themselves.

3.1   Dark reaction production of I_2

After the initial connection of the flowtube to the CIMS (i.e., before irradiation or addition of O_3), large I_2 signals (measured as I_3^-, m/z 381) were observed in several cases where OH-radical precursors were utilized, especially when pH $\leq$ 2 (e.g., Fig. 2b, Fig. S2). Integrated calibrated sums of this dark I_2 production are estimated in Table S1, and span from the time when the flowtube was connected to the CIMS until lights were activated. When pH $\leq$ 2, dark production of I_2 sometimes caused significant depletion of reservoir I^-. Experiments IO4 and SW5 (both using H_2O_2 as an OH precursor) only had, at most, ~36% of the initial 152 nmol of I^- by the time lights were turned on (remaining I^- was estimated by subtracting twice the observed I_2 (i.e., two I^- for every I_2) from the initial 152 nmol of I^- in the IO

257 or SW solutions). Considerably less dark I_2 production occurred using NO_2^- as an OH precursor (depleting I^- by an

258 average of 4.5%, Table S1). However, the amounts in Table S1 represent lower limits of the dark-produced I_2; it is

259 impossible to accurately determine the extent of dark I_2 production since some was lost from the flow tube during its

260 connection to the CIMS after freezing (Fig. 1). At pH $\approx$ 4.7, this production was relatively modest. Only experiment

261 IO2 was noticeably affected, in which only ~0.5% of initial I^- was removed by dark mechanisms (Table S1). Under

262 both pH regimes (i.e. ~4.7 and < 2), this signal subsequently decayed as I_2 flushed out of the system until reaching a

263 low steady state concentration. No corresponding dark production of Br_2 or Cl_2 was observed for any experiments at

264 any pH.

265   As previously reported, both H_2O_2 and NO_2^- can directly convert I^- to I_2 under dark acidic conditions. The

266 oxidation of I^- by H_2O_2 occurs through the condensed phase reactions R23 and R24 (Küpper et al., 1998):

267 $I^- + H_2O_2 \leftrightarrow HOI + OH^-$ $\qquad\qquad\qquad\qquad\qquad\qquad\qquad\qquad\qquad$ (R23)

268 $HOI + I^- + H^+ \rightarrow I_2 + H_2O$ $\qquad\qquad\qquad\qquad\qquad\qquad\qquad\qquad\qquad$ (R24)

269 Nitrite ions react with hydronium ions to form the nitroacidium ion, H_2ONO^+, which has been previously shown to

270 produce I_2 (R25-R27) (Hellebust et al., 2007; O'Driscoll et al., 2006, 2008; O'Sullivan and Sodeau, 2010):

271 $NO_2^- + H_3O^+ \leftrightarrow HONO + H_2O$ $\qquad\qquad\qquad\qquad\qquad\qquad\qquad\qquad$ (R25)

272 $HONO + H_3O^+ \leftrightarrow H_2ONO^+ + H_2O$ $\qquad\qquad\qquad\qquad\qquad\qquad\qquad$ (R26)

273 $2\,H_2ONO^+ + 2I^- \leftrightarrow 2NO + I_2 + 2H_2O$ $\qquad\qquad\qquad\qquad\qquad\qquad\qquad$ (R27)

274 Therefore, it is likely the I_2 observed on connection of the flowtube to CIMS originated from the above reactions

275 (R23-27), as the pH $\leq$ 2 experiments in this work (IO3-5, SW3-5) favor these forward reactions.

276 **3.2   Hydroxyl radical-induced halogen production**

277 **3.2.1   pH $\approx$ 4.7**

278   At pH $\approx$ 4.7, frozen solutions without OH radical precursors produced no (IO6, SW6-SW7) or little (IO7,

279 0.10 $\pm$0.06 nmol of I_2) amounts of molecular halogens above their respective LODs after activation of lights (Table

280 2). The small amount of I_2 produced in IO7 possibly originates from the light and O_2-mediated production mechanism

281 proposed by Kim et al. (2016) as summarized within R13-R17. However, as shown below, this mechanism of I_2

282 production is of relatively minor importance at this pH.

283   In the presence of H_2O_2 at pH $\approx$ 4.7, I_2 mole fractions increased rapidly upon irradiation, as shown in Fig. 2a.

284 Of the four experiments performed in these conditions (IO1, IO2, SW1, SW2), three experiments (IO1, SW1, SW2)

285 produced statistically similar amounts of I_2 (mean: 8 $\pm$ 2 nmol) after one hour of irradiation (Table 2). The I_2 signal

286 behavior in Experiment IO2 qualitatively shared the same features as Experiments IO1, SW1, and SW2 (Fig. S3), but

287 provided an apparently statistically different amount of I_2 (0.6 ($\pm$0.4) nmol) based on the objectively chosen integration

288 limits. This experiment is discussed further in the Supplemental Information.

289   Regarding other molecular halogens, IBr was observed above the estimated limits of detection (3 pmol

290 mol^{-1}) upon irradiation during Experiment SW2 (Fig. 2a), starting approximately 20 minutes before the addition of

291 O_3. No photochemically produced (OH-induced) Br_2 was unambiguously observed at this pH (note that the apparent

292 IO2 Br_2 production of 0.034 $\pm$ 0.003 nmol is likely overestimated and discussed in more detail in the Supplemental

293 Information). Cl_2 mole fractions remained below limits of detection in all cases with OH-precursors at this pH.

294 **3.2.2 pH $\leq$ 2**

295   In cases without OH precursors at pH $\leq$ 2, photochemical I_2 production was observed (integrated production

296 of 14 $\pm$ 10 nmol for IO8, and 6 $\pm$ 2 nmol for SW8) (Table 2), contrasting with experiments performed at pH $\approx$ 4.7 in

297 which very little was produced. This production likely stems from the mechanisms outlined by Kim et al. (2016)

298 (R13-17), which requires only light and oxygen to form a charge-transfer complex that results in I_2 production

299 (discussed in Sect. 1). Molecular Br_2 and Cl_2 concentrations remained below limits of detection, consistent with

300 Abbatt et al. (2010), in which no Br_2 or Cl_2 was observed without an OH-precursor.

301   As discussed in Sect. 3.1, inclusion of H_2O_2 or NO_2^- can result in direct oxidation of I^- and reduce the available

302 [I^-] for photochemical OH oxidation when pH $\leq$ 2. Photochemical production of I_2 across experiments yielded $\leq$ 0.82

303 nmol (IO4, IO5, and SW5) when H_2O_2 was used as an OH precursor. However, when instead NO_2^- was used (as in

304 IO3, SW3, and SW4), initial observations of I_2 on flowtube connection to CIMS were as much as 90% less than when

305 H_2O_2 was used (Table S1), thereby leaving more I^- available for reaction. For experiment IO3 (using NO_2^-), the

306 reduced pH led to an observed photochemical I_2 production amount of 39 $\pm$ 1 nmol, approximately four times larger

307 than the largest amount observed at pH $\approx$ 4.7 (9 $\pm$ 3 nmol, Table 2). That production would be enhanced at lower pH

308 was expected based on the halogen activation reactions R4-R22. The corresponding "saltwater" experiments using

309 NO_2^- were not as conclusive; experiment SW3 only yielded 4.0 $\pm$ 0.1 nmol of photochemical I_2 (Fig. S5). Experiment

310   SW4 (a repeat of SW3) did not produce any photochemical I_2 and qualitatively resembles the H_2O_2 experiments

311   performed at this pH. It is possible that, for SW3 and SW4, more I_2 was produced by dark reactions and flushed out

312   of the tube during connection with the CIMS and therefore would not have been measured.

313   Photochemical production of Br_2 does not appear until I_2 production decreases. The results shown in Figures

314   2a and 2b demonstrate that when $[I^-]/[Br^-]$ approximates the initial conditions of Instant Ocean (~2.6 x 10^{-3}), OH-

315   mediated I_2 production precedes Br_2 and IBr production (as in the pH $\approx$ 4.7 experiments and IO3, in which significant

316   dark I_2 production was not observed). After $[I^-]/[Br^-]$ has sufficiently decreased, Br_2 eventually becomes the dominant

317   photochemical product. As demonstrated by experiment IO4 (Fig 2b and inset), there is a delay in Br_2 production

318   until I^- was removed as I_2, then as IBr. For experiments that used H_2O_2, photochemical Br_2 yields averaged 4.5 $\pm$ 0.5

319   nmol between IO4 and IO5, and 6.0 $\pm$ 0.7 nmol from SW5. Experiment SW4 (using NO_2^-) produced a comparable

320   amount of Br_2 (5.4 $\pm$ 0.7 nmol). Given the initial depletion of I^- from dark I_2 production (Sect. 3.1), we can estimate

321    $[I^-]/[Br^-]$ at pH $\leq$ 2 in ice with H_2O_2 just before irradiation based on the remaining moles of I^- in solution (Table S1)

322   and the total moles of Br^- in the solution. Averaging values from Experiments IO4-5 and SW5, $[I^-]/[Br^-]$ was calculated

323   as (1.6 $\pm$ 0.7) x 10^{-4} (compared to the initial ratio of 2.6 x 10^{-3}) and was sufficiently low to result in photochemical

324   production of Br_2.

325   Photochemical Cl_2 production was only observed from a frozen solution of "pure" 0.56 M NaCl and H_2O_2 at

326   pH=1.8 (CL1), as shown in Fig. 2c. The initial Br^- impurity of this CL1 solution was determined to be (4.5 $\pm$ 0.3) x

327   10^{-6} M via ion chromatography, while any I^- impurity concentration could not be detected above the 3σ LOD of 90

328   nM. When the lights were turned on, slight increases in I_2 and IBr were observed in concert with a rapid rise in Br_2.

329   After about one hour of apparent equilibrium, I_2 concentrations began decreasing, while Br_2, IBr, and Cl_2 continued

330   rising. Over one hour of illumination, 93 $\pm$ 3 pmol of Cl_2, 100 $\pm$ 10 pmol of Br_2, and 100 $\pm$ 10 pmol of I_2 were observed.

331   However, as shown in Fig 2c, the greatest rate of increase in Cl_2 signal occurred just after this time. Integrating instead

332   from t=0 until t=2 hours, the amount of Cl_2 produced was 190 $\pm$ 10 pmol, while the amount of Br_2 increased to 310 $\pm$

333   20 pmol. Utilizing the starting halide concentrations of Br^- and Cl^- for CL1, our results show Cl_2 production was

334   observed at $[Br^-]/[Cl^-]$ of 8.1 x 10^{-6} ($^1/_{124,000}$), compared to the Instant Ocean $[Br^-]/[Cl^-]$ of ~ $^1/_{800}$. Unfortunately, BrCl

335   could not be observed due to an unknown interference at m/z 241 and 243.

336   The observations in this study indicate competition for the OH radical in which the most oxidizable halide is

337   oxidized, and the corresponding molecular halogens are produced until that halide ion is depleted in the ice surface

338 brine reaction environment. The trends in molecular halogen production confirm acid-enhanced mechanisms in which

339 the dominant products are largely dependent on relative halide ratios. Here, Br_2 and IBr were not observed until I_2

340 production sufficiently decreased the $[I^-]/[Br^-]$ ratio, and Cl_2 was not observed unless the $[Br^-]/[Cl^-]$ ratio was

341 sufficiently low ($[Br^-]/[Cl^-] = 8.1$ x 10^{-6}, as discussed above). This observation is consistent with Sjostedt and Abbatt

342 (2008), who exposed frozen salt solutions to gas-phase OH and found peak BrCl production occurred as Br^- decreased

343 from an initial $[Br^-]/[Cl^-]$ of 7.3 x 10^{-5}. Additionally, Abbatt et al. (2010) generated condensed phase OH on frozen

344 surfaces via the photolysis of nitrate, and similarly found lower Br_2 and IBr integrated amounts at lower $[Br^-]/[Cl^-]$

345 when temperatures were higher than the eutectic point of sodium chloride. These halide ratios are also consistent with

346 in situ snowpack observations of Br_2, BrCl, and Cl_2 formation (Custard et al., 2017; Pratt et al., 2013).

347 **3.2.3 Relative Reactivites of OH-induced Halogen Production**

348 I_2, Br_2, and Cl_2 have been previously observed at mole fractions within less than two orders of magnitude of

349 each other in snowpack interstitial air at Utqiaġvik, AK, (Custard et al., 2017; Raso et al., 2017). Custard et al. (2017)

350 observed gas phase $[Br_2]/[Cl_2]$ values for artificially irradiated, acidic snowpacks ranging from 2-95 for corresponding

351 snowpack $[Br^-]/[Cl^-]$ ratios of (6 ± 1) x 10^{-4}. Under similar conditions, Raso et al. (2017) observed $[I_2]/[Br_2]$ ranging

352 from ~0.4-0.8 from corresponding snowpack $[I^-]/[Br^-]$ amounts of (2.6 ± 0.6) x 10^{-3}. Despite the large differences in

353 relative halide abundance (i.e., $[I^-] << [Br^-] << [Cl^-]$), it appears that halogen activation reaction kinetics favor the

354 larger halide ions, effectively levelling the relative molecular halogen production rates. The observations herein

355 provide an opportunity to explore the relative reactivities of OH-mediated halogen production.

356 If we assume that the observed X_2 flux out of the ice is proportional to the production rate (i.e., X_2 desorbs

357 as it is produced, within the residence time of the flow tube) and that halogen production is limited by halide reaction

358 with OH radicals, effective relative reactivities, k_{X^-}/k_{Y^-}, (where X and Y represent Br, Cl, or I) can be calculated using

359 Eq. 1.

360 $$\frac{Flux_{X_2}}{Flux_{Y_2}} = \frac{k_{X^-}[X^-][OH][H^+]}{k_{Y^-}[Y^-][OH][H^+]} \qquad (1)$$

361 The initial molecular halogen flux is calculated as the integrated sum of X_2 (in moles) divided by both integration time

362 (t = 0-3 minutes, starting from the beginning of irradiation) and the surface area of ice coverage in the flow tube.

363 Because the surface area, as well as the [OH] and $[H^+]$ in the ice surface reaction environment, are identical within

364 individual experiments and cancel in these calculations the relative fluxes are simply equivalent to the relative outflow

365 concentrations of halogens. The pre-freezing halide ion concentrations (defined in Sect. 2) thus allow us to solve for

366 the effective relative reactivity, k_{X^-}/k_{Y^-} by assuming the ratios of the halide ice concentrations are the same after

367 freezing.

368   At pH = 1.8, k_{Br^-}/k_{Cl^-} was estimated to be $(2.4 \pm 0.2) \times 10^5$ from experiment CL1; in other words, production

369 of Br_2 is 240,000 times more efficient than production of Cl_2 via (OH + halide) in the surface layer. Across the six

370 experiments performed at pH ≤ 2 (average of 1.85) using Instant Ocean (IO3, IO4, IO5) and saltwater (SW3, SW4,

371 SW5), k_{I^-}/k_{Br^-} was calculated to average $(9 \pm 4) \times 10^3$ (reported uncertainty is the standard error of the mean, and thus

372 only represents the experiment repeatability).   These relative reactivities are substantially larger than the

373 corresponding relative aqueous OH + halide rate constants ($k_{I^-} = k_{Br^-} = 1.1 \times 10^{10}$ M^{-1} s^{-1} (Buxton et al., 1988; Zehavi

374 and Rabani, 1972), $k_{Cl^-} = 3.0 \times 10^9$ M^{-1} s^{-1} (Grigor'ev et al., 1987)), which are different by less than a factor of 4.

375 However, these rate constants refer to the specific fundamental reaction of OH with X^- to produce HOX^-, as in Reaction

376 R8. Ultimately, X_2 production would occur via R8-R12, and this condensed phase chemistry is much more complex

377 when also considering interhalogen reactions, such as R28, that involve combinations of the three molecular halogens,

378 halides, and mixed molecular halogens (XY, where Y = Cl, Br, or I).

379   XY   + X^- → X_2 + Y^- (R28)

380 Thus, it must be that there exist competing reactions that make the production of the larger X_2 more efficient. For

381 example, $Cl + I^- \rightarrow ClI^-$ may be faster than $Cl + Cl^- \rightarrow Cl_2^-$. Alternatively, the relative rates of the disproportionation

382 reaction R11 are likely different, favoring the larger molecular halogens. We can thus only state from these

383 observations that the apparent relative reactivities calculated are consistent with the overall reactivity of the larger

384 ions compensating for their lower abundances. This may lead to comparable production rates in our laboratory

385 experiments and comparable snowpack gas phase concentrations.

386   The above relative reactivity calculations are considered upper limits since the halide ratios used represent

387 those in the pre-freezing solution. In other words, it is assumed that the ions are excluded to the ice surface reaction

388 environment-air interface in amounts proportional to their pre-freezing concentration. Malley et al. (2018) recently

389 demonstrated that brine can be distributed throughout ice in channels, suggesting that only the solutes at the liquid-air

390 interface (a fraction of the total pre-freezing solution) participate in heterogeneous chemistry. Indeed, we find

391 evidence here suggesting not all ions are available for reaction at the ice brine surface, particularly for experiments

392 for which little I⁻ was lost from dark I_2 production mechanisms (i.e., pH = 4.7 with OH precursors: IO1, IO2, SW1,

393 SW2). Considering experiment IO2 as an example (Fig. S5; pH = 4.7), integration of the I_2 signal during ~15 hours

394 of exposure to both light and O_3 shows that 54% (82 nmol) of the original 152 nmol of I⁻ remained unreacted in the

395 frozen solution despite the signal apparently stabilizing at its baseline. It is therefore probable that a significant number

396 of the ions, as well as H_2O_2, exist within brine channels within the ice (Bartels-Rausch et al., 2014; Malley et al.,

397 2018). Oxidation chemistry would then be occurring throughout the ice, but release of molecular halogens to the flow

398 tube air would be determined by diffusion rates. The diffusion rates of the product molecular halogens through bulk

399 ice are likely slow, such that only production occurring in the brine that is in the near-liquid-air interface is observed

400 here (Abbatt et al., 2012). Of the halogens produced from frozen solutions here, it is expected that I_2 is observed most

401 readily given the high polarizability and surface affinity of I⁻ in aqueous solutions (Gladich et al., 2011), and the

402 relative ease of oxidation of I⁻. That is, surface concentrations will be relatively enhanced with larger, more polarizable

403 anions (I⁻ > Br⁻ > Cl⁻) (Gladich et al., 2011), which favors production of I_2 over Br_2, and Br_2 over Cl_2. As the

404 larger/more reactive ions are depleted through oxidation, the next largest ion then becomes more favorably oxidized.

405 Thus, in addition to the impact of differential reactivities and competing reactions for R9-R12, what we observe in the

406 laboratory and in the field can also be influenced by the relative surface enhancements of the anions, especially with

407 respect to O_3 impacts as discussed below.

3.3   Effects of O_3 on halogen production

409   In experiments without an OH source (IO6-IO8, SW6-SW8), I_2 production was greatest when O_3 was

410 introduced to the irradiated tube for both pH regimes (Table 2). The amount of I_2 produced over 60 minutes in these

411 experiments was large, ranging from 26 ± 9 nmol to 80 ± 1 nmol at pH = 4.7, and from 2.6 ± 1.7 nmol to 38 ± 12 nmol

412 at pH < 2. This production likely results from a combination of heterogeneous recycling, and the surface and aqueous

413 reactions between O_3 and I⁻ (k = 2.0×10^{-12} cm^3 molecules^{-1} s^{-1} (Liu et al., 2001)). While the I_2 produced when pH <

414 2 appears to be lower, I_2 had already been produced in the presence of light prior to addition of O_3 (Sect. 3.2.2),

415 yielding a lower [I⁻]/[Br⁻] ratio when O_3 was eventually added. Br_2 production amounts ranged from 0.012 ± 0.001

416 nmol to 0.16 ± 0.01 nmol at pH = 4.7 and taking up to 6 hours to raise above detection limits after O_3 was added. At

417 pH ≤ 2, Br_2 production amounts ranged 0.14 ± 0.02 nmol to 0.93 ± 0.05 nmol. While O_3-mediated halogen production

418   has been observed directly from frozen surfaces in the absence of light in previous laboratory studies (Artiglia et al.,

419   2017; Oldridge and Abbatt, 2011; Oum et al., 1998a; Wren et al., 2013), Br_2 production has not been directly observed

420   from the Arctic snowpack without irradiation (Pratt et al., 2013). This raises a question of the role of O_3 in initial

421   halogen release in the Arctic spring.

422   When OH-precursors were present, the addition of O_3 to the zero-air flow over the irradiated frozen sample

423   caused additional production of I_2 and Br_2, as shown in Figure 2a and b, under both pH regimes (Table 2). In

424   experiments at pH $\approx$ 4.7 in which [I^-]/[Br^-] remained sufficiently large due to minimal dark production of I_2 (i.e., IO1-

425   2, SW1-2), exposure to O_3 caused a sharp increase in I_2 (as in Fig. 2a). I_2 production amounts for frozen Instant Ocean

426   at pH $\approx$ 4.7 (IO1, IO2) averaged 22 ± 10 nmol, about two times less than for frozen saltwater experiments SW1 and

427   SW2 (average production amount of 51 ± 25 nmol). As the I_2 signal decayed, the corresponding Br_2 signals gradually

428   increased above detection limits, approximately 3h after the introduction of O_3 (Fig. 2a). The average integrated

429   amounts of Br_2 produced from these pH $\approx$ 4.7 experiments were very similar (0.05 ± 0.01 nmol for IO experiments

430   and 0.03 ± 0.01 nmol for SW experiments).

431   When pH $<$ 2, the effects of O_3 addition varied according to the remaining availability of I^-. When the surface

432   I^- reservoir had been reduced from dark reactions with H_2O_2 or NO_2^- (R17-21; Sect. 3.1), exposure to O_3 did not

433   increase I_2 above the LOD except in experiment IO5, which exhibited a small spike before decaying below the LOD

434   (0.11 ± 0.06 nmol in IO5). However, O_3 did cause additional Br_2 production after one hour (average of 10 ± 2 nmol

435   for IO4 (Fig. 2b) and IO5 (Fig S4), and 14 ± 2 nmol for SW4 and SW5). In contrast, for SW3 (using NO_2^- as an OH

436   source), there was relatively little initial consumption of I^- by dark reaction; therefore, when O_3 was added, 1.1 ± 0.1

437   nmol additional I_2 was observed, comparable to what was observed with the higher pH experiments (Fig. S5). The

438   amount of Br_2 produced (0.46 ± 0.01 nmol) was also significantly less than observed when I^- was initially depleted,

439   demonstrating the importance of the halide ratios.

440   This additional O_3-induced halogen production could result from a combination of mechanisms. First, as

441   discussed above, O_3 can react with halides on frozen saline surfaces to produce Br_2 or I_2 per reactions R18-19, and

442   then R4 (Artiglia et al., 2017; Carpenter et al., 2013; Gladich et al., 2015; Hayase et al., 2010; Oum et al., 1998a;

443   Shaw and Carpenter, 2013; Wren et al., 2013). It is possible that Br_2 (as well as other halogens) may have been

444   produced via this mechanism at levels below the LOD in previous Arctic snowpack studies (Custard et al., 2017; Pratt

445   et al., 2013; Raso et al., 2017).

446   The presence of O_3 also yielded HOX compounds (Fig. 3-4), likely formed in the flowtube in part by O_3

447   reactions with halides (R18-R19). Additionally, given a flow tube residence time of 12 seconds, gas phase production

448   of HOX is possible via R1-R3 and could act as an additional X_2 production source (via R4), given a timescale for

449   molecular diffusion of 6.5 seconds for HOBr from the center of the tube to the ice surface. At this flow rate, there is

450   enough time for 1-2 heterogeneous reaction cycles. Figure 3 shows HOX for IO2 (pH=4.7 with H_2O_2 present,

451   analogous to IO1, SW1, SW2). For each experiment in this series, increases in I_2, HOI, and Br_2 were readily observed

452   when the O_3 was introduced at hour 2 (Fig. 3, Fig. S4). However, corresponding HOBr production was not observed,

453   perhaps either due to a high LOD, or the relatively low abundance of Br_2 that would limit production of HOBr.

454   Conversely, in pH $\leq$ 2 cases when substantial portions of I$^-$ had already reacted prior to irradiation (IO4, IO5, SW4,

455   SW5), the addition of O_3 produced negligible amounts of I_2 and HOI (Fig. 4). But, in these cases, following the

456   addition of O_3, HOBr (m/z 225 IHO^{81}Br$^-$), was observed together with Br_2 (Fig. 4, Fig. S4). We note in this case that

457   m/z 223, representative of IHO^{79}Br$^-$, does not appear to show an enhancement when O_3 is added to the system. There

458   was a much higher background signal for m/z 223 compared with m/z 225 (IHO^{81}Br$^-$) resulting from an unknown

459   interference.

460   4   **Summary and Conclusions**

461   It was shown in this ice-coated wall flow tube laboratory study that the hydroxyl radical can act as an effective

462   condensed-phase halide oxidant leading to I_2, IBr, Br_2, and Cl_2 production under acidic conditions. Rates of molecular

463   halogen production and release were dictated by both pH and relative halide concentrations. The identities of the

464   molecular halogens produced appears to be highly influenced by which ions are enhanced at the ice surface, with I_2

465   production occurring prior to Br_2 production, which commenced as the [I$^-$]/[Br$^-$] was reduced. An opportunity exists

466   to further explore this chemistry via surface-sensitive methods, for which recent developments have been shown to

467   effectively enable characterization of the surface composition of frozen solutions of sodium chloride under near

468   atmospherically relevant conditions (Artiglia et al., 2017; Orlando et al., 2016). It would be useful to confirm the

469   dominant ions involved in this surface-based chemistry over time. Further investigations into the effects of halide

470   ratios on halogen production are also suggested, including measurements of how the ratios vary for different frozen

471   Arctic surfaces, as well as how they vary spatially. While condensed-phase OH produces Br_2 and I_2 most rapidly in

472   this study, it appears that other mechanisms, such as heterogeneous recycling of HOCl or ClONO$_2$, could be a more

473   dominant mechanism for in situ production of gas phase Cl$_2$ (Wang and Pratt, 2017). We find the addition of gas phase

474   O$_3$ produces additional Br$_2$ and I$_2$, likely through aqueous reactions with halides and/or gas-phase production of HOX

475   or possibly XONO$_2$ (Deiber et al., 2004) and subsequent halogen explosion chemistry. These results lend support for

476   the photochemical, condensed-phase molecular halogen production mechanisms proposed by the recent in situ

477   snowpack experiments (Custard et al., 2017; Pratt et al., 2013; Raso et al., 2017).

478   Understanding the environmental pH-dependence of halogen activation necessitates study of the pH on

479   relevant Arctic frozen surfaces. Pratt et al. (2013) found that the frozen surfaces most conducive to in-situ

480   photochemical Br$_2$ production had acidic pH after melting, while no production was observed from those with a well-

481   buffered alkaline ice brine. Similarly, we find herein that condensed-phase OH-induced halogen production is

482   enhanced at lower pH. Wren and Donaldson (2012a, 2012b) found in laboratory studies that pH of acidic and basic

483   solutions remains essentially unchanged after freezing, and that saline solutions with buffers (i.e., seawater) maintain

484   their buffering capacity following trace gas deposition, supporting the lack of observed Br$_2$ production from the sea

485   ice surface (Pratt et al., 2013). Therefore, it would be useful to test in-situ production of halogens from Arctic frozen

486   surfaces in tandem with measurement of the pH of said surfaces to determine the atmospherically relevant surface pH

487   range required for halogen production.

488

489   *Data availability*. Halfacre, J. W., Shepson, P. B., Pratt, K. A.: Laboratory experiments of the pH-dependent

490   production of molecular chlorine, bromine, and iodine from frozen saline surfaces, NSF Arctic Data Center,

491   http://dx.doi.org/10.18739/A22804Z17, 2018

492

493   *Author contributions*. JWH and PBS designed the research and JWH performed the experiments and data

494   analysis. All three authors contributed to the discussion and interpretation of the results and writing of the paper.

495

496   *Competing interests*. The authors declare that they have no conflict of interest.

Acknowledgements

We thank the National Science Foundation for their funding (PLR-1417668 and PLR-1417906, OPP-1417668). We also express thanks to J. H. Slade, L. G. Huey, D. J. Tanner, F. Xiong, A. R. W. Raso, and K. D. Custard for their assistance with CIMS operation and maintenance. Additionally, we thank the Purdue Chemistry Shop for helping build both the cooling and photolysis boxes, as well as the Jonathan Amy Facility for Chemical Instrumentation for their support in the fabrication of the experimental flow tube and setup of our experimental boxes. Thanks are also extended to M. Haas and M. Bischoff for performing total organic carbon analysis of our samples, and A. R. W. Raso for confirmation of the iodide concentrations in our Instant Ocean samples. Finally, we thank T. Miller and the Purdue Birck Nanotechnology Center for the provision of the nano-grade water used for our samples.

References

Abbatt, J., Oldridge, N., Symington, A., Chukalovskiy, V., McWhinney, R. D., Sjostedt, S. and Cox, R. A.: Release of Gas-Phase Halogens by Photolytic Generation of OH in Frozen Halide−Nitrate Solutions: An Active Halogen Formation Mechanism?, J. Phys. Chem. A, 114(23), 6527–6533, doi:10.1021/jp102072t, 2010.

Abbatt, J. P. D., Thomas, J. L., Abrahamsson, K., Boxe, C., Granfors, A., Jones, A. E., King, M. D., Saiz-Lopez, A., Shepson, P. B., Sodeau, J., Toohey, D. W., Toubin, C., von Glasow, R., Wren, S. N. and Yang, X.: Halogen activation via interactions with environmental ice and snow in the polar lower troposphere and other regions, Atmos Chem Phys, 12(14), 6237–6271, doi:10.5194/acp-12-6237-2012, 2012.

Artiglia, L., Edebeli, J., Orlando, F., Chen, S., Lee, M.-T., Corral Arroyo, P., Gilgen, A., Bartels-Rausch, T., Kleibert, A., Vazdar, M., Andres Carignano, M., Francisco, J. S., Shepson, P. B., Gladich, I. and Ammann, M.: A surface-stabilized ozonide triggers bromide oxidation at the aqueous solution-vapour interface, Nat. Commun., 8(1), doi:10.1038/s41467-017-00823-x, 2017.

Barrie, L. and Platt, U.: Arctic tropospheric chemistry: an overview, Tellus B, 49(5), 450–454, doi:10.1034/j.1600-0889.49.issue5.2.x, 1997.

Bartels-Rausch, T., Jacobi, H.-W., Kahan, T. F., Thomas, J. L., Thomson, E. S., Abbatt, J. P. D., Ammann, M., Blackford, J. R., Bluhm, H., Boxe, C., Domine, F., Frey, M. M., Gladich, I., Guzmán, M. I., Heger, D., Huthwelker, T., Klán, P., Kuhs, W. F., Kuo, M. H., Maus, S., Moussa, S. G., McNeill, V. F., Newberg, J. T., Pettersson, J. B. C.,

Roeselová, M. and Sodeau, J. R.: A review of air–ice chemical and physical interactions (AICI): liquids, quasi-liquids, and solids in snow, Atmos Chem Phys, 14(3), 1587–1633, doi:10.5194/acp-14-1587-2014, 2014.

Buxton, G. V., Greenstock, C. L., Helman, W. P. and Ross, A. B.: Critical Review of rate constants for reactions of hydrated electrons, hydrogen atoms and hydroxyl radicals ($\cdot$OH/$\cdot$O$^-$ in Aqueous Solution, J. Phys. Chem. Ref. Data, 17(2), 513–886, doi:10.1063/1.555805, 1988.

Carpenter, L. J., MacDonald, S. M., Shaw, M. D., Kumar, R., Saunders, R. W., Parthipan, R., Wilson, J. and Plane, J. M. C.: Atmospheric iodine levels influenced by sea surface emissions of inorganic iodine, Nat. Geosci., 6(2), 108–111, doi:10.1038/ngeo1687, 2013.

Cho, H., Shepson, P. B., Barrie, L. A., Cowin, J. P. and Zaveri, R.: NMR Investigation of the Quasi-Brine Layer in Ice/Brine Mixtures, J. Phys. Chem. B, 106(43), 11226–11232, doi:10.1021/jp020449+, 2002.

Custard, K. D., Pratt, K. A., Wang, S. and Shepson, P. B.: Constraints on Arctic Atmospheric Chlorine Production through Measurements and Simulations of Cl $_2$ and ClO, Environ. Sci. Technol., 50(22), 12394–12400, doi:10.1021/acs.est.6b03909, 2016.

Custard, K. D., Raso, A. R. W., Shepson, P. B., Staebler, R. M. and Pratt, K. A.: Production and Release of Molecular Bromine and Chlorine from the Arctic Coastal Snowpack, ACS Earth Space Chem., 1(3), 142–151, doi:10.1021/acsearthspacechem.7b00014, 2017.

Deiber, G., George, C., Calvé, S. L., Schweitzer, F. and Mirabel, P.: Uptake study of ClONO$_2$ and BrONO$_2$ by Halide containing droplets, Atmospheric Chem. Phys., 4(5), 1291–1299, doi:https://doi.org/10.5194/acp-4-1291-2004, 2004.

Fickert, S., Adams, J. W. and Crowley, J. N.: Activation of Br2 and BrCl via uptake of HOBr onto aqueous salt solutions, J. Geophys. Res. Atmospheres, 104(D19), 23719–23727, doi:10.1029/1999JD900359, 1999.

France, J. L., Reay, H. J., King, M. D., Voisin, D., Jacobi, H. W., Domine, F., Beine, H., Anastasio, C., MacArthur, A. and Lee-Taylor, J.: Hydroxyl radical and NO $_x$ production rates, black carbon concentrations and light-absorbing impurities in snow from field measurements of light penetration and nadir reflectivity of onshore and offshore coastal Alaskan snow, J. Geophys. Res., 117, doi:10.1029/2011JD016639, 2012.

Garland, J. A. and Curtis, H.: Emission of iodine from the sea surface in the presence of ozone, J. Geophys. Res., 86(C4), 3183, doi:10.1029/JC086iC04p03183, 1981.

Gladich, I., Shepson, P. B., Carignano, M. A. and Szleifer, I.: Halide Affinity for the Water−Air Interface in Aqueous Solutions of Mixtures of Sodium Salts, J. Phys. Chem. A, 115(23), 5895–5899, doi:10.1021/jp110208a, 2011.

551 Gladich, I., Francisco, J. S., Buszek, R. J., Vazdar, M., Carignano, M. A. and Shepson, P. B.: Ab Initio Study of the

552 Reaction of Ozone with Bromide Ion, J. Phys. Chem. A, 119(19), 4482–4488, doi:10.1021/jp5101279, 2015.

553 Grigor'ev, A. E., Makarov, I. E. and Pikaev, A. K.: Formation of Cl_2^- in the bulk of solution during radiolysis of

554 concentrated aqueous solutions of chlorides, Khimiya Vysok. Ehnergij, 21(2), 123–126, 1987.

555 Hayase, S., Yabushita, A., Kawasaki, M., Enami, S., Hoffmann, M. R. and Colussi, A. J.: Heterogeneous Reaction of

556 Gaseous Ozone with Aqueous Iodide in the Presence of Aqueous Organic Species, J. Phys. Chem. A, 114(19), 6016–

557 6021, doi:10.1021/jp101985f, 2010.

558 Hellebust, S., Roddis, T. and Sodeau, J. R.: Potential Role of the Nitroacidium Ion on HONO Emissions from the

559 Snowpack, J. Phys. Chem. A, 111(7), 1167–1171, doi:10.1021/jp068264g, 2007.

560 Herring, J. R. and Liss, P. S.: A new method for the determination of iodine species in seawater, Deep Sea Res.

561 Oceanogr. Abstr., 21(9), 777–783, doi:10.1016/0011-7471(74)90085-0, 1974.

562 Kim, K., Yabushita, A., Okumura, M., Saiz-Lopez, A., Cuevas, C. A., Blaszczak-Boxe, C. S., Min, D. W., Yoon, H.-

563 I. and Choi, W.: Production of Molecular Iodine and Tri-iodide in the Frozen Solution of Iodide: Implication for Polar

564 Atmosphere, Environ. Sci. Technol., 50(3), 1280–1287, doi:10.1021/acs.est.5b05148, 2016.

565 Knipping, E. M., Lakin, M. J., Foster, K. L., Jungwirth, P., Tobias, D. J., Gerber, R. B., Dabdub, D. and Finlayson-

566 Pitts, B. J.: Experiments and Simulations of Ion-Enhanced Interfacial Chemistry on Aqueous NaCl Aerosols, Science,

567 288(5464), 301–306, doi:10.1126/science.288.5464.301, 2000.

568 Küpper, F. C., Schweigert, N., Gall, E. A., Legendre, J.-M., Vilter, H. and Kloareg, B.: Iodine uptake in Laminariales

569 involves   extracellular,   haloperoxidase-mediated   oxidation   of   iodide,   Planta,   207(2),   163–171,

570 doi:10.1007/s004250050469, 1998.

571 Liao, J., Huey, L. G., Tanner, D. J., Flocke, F. M., Orlando, J. J., Neuman, J. A., Nowak, J. B., Weinheimer, A. J.,

572 Hall, S. R., Smith, J. N., Fried, A., Staebler, R. M., Wang, Y., Koo, J.-H., Cantrell, C. A., Weibring, P., Walega, J.,

573 Knapp, D. J., Shepson, P. B. and Stephens, C. R.: Observations of inorganic bromine (HOBr, BrO, and Br_2) speciation

574 at Barrow, Alaska, in spring 2009, J. Geophys. Res. Atmospheres, 117(D14), D00R16, doi:10.1029/2011JD016641,

575 2012.

576 Liao, J., Huey, L. G., Liu, Z., Tanner, D. J., Cantrell, C. A., Orlando, J. J., Flocke, F. M., Shepson, P. B., Weinheimer,

577 A. J., Hall, S. R., Ullmann, K., Beine, H. J., Wang, Y., Ingall, E. D., Stephens, C. R., Hornbrook, R. S., Apel, E. C.,

578   Riemer, D., Fried, A., Mauldin Iii, R. L., Smith, J. N., Staebler, R. M., Neuman, J. A. and Nowak, J. B.: High levels

579   of molecular chlorine in the Arctic atmosphere, Nat. Geosci., 7(2), 91–94, doi:10.1038/ngeo2046, 2014.

580   Liu, Q., Schurter, L. M., Muller, C. E., Aloisio, S., Francisco, J. S. and Margerum, D. W.: Kinetics and Mechanisms

581   of Aqueous Ozone Reactions with Bromide, Sulfite, Hydrogen Sulfite, Iodide, and Nitrite Ions, Inorg. Chem., 40(17),

582   4436–4442, doi:10.1021/ic000919j, 2001.

583   Lockwood, A. L., Shepson, P. B., Fiddler, M. N. and Alaghmand, M.: Isoprene nitrates: preparation, separation,

584   identification, yields, and atmospheric chemistry, Atmos Chem Phys, 10(13), 6169–6178, doi:10.5194/acp-10-6169-

585   2010, 2010.

586   Luther, G. W., Swartz, C. B. and Ullman, W. J.: Direct determination of iodide in seawater by cathodic stripping

587   square wave voltammetry, Anal. Chem., 60(17), 1721–1724, doi:10.1021/ac00168a017, 1988.

588   Malley, P. P. A., Chakraborty, S. and Kahan, T. F.: Physical Characterization of Frozen Saltwater Solutions Using

589   Raman Microscopy, ACS Earth Space Chem., doi:10.1021/acsearthspacechem.8b00045, 2018.

590   McConnell, J. C., Henderson, G. S., Barrie, L., Bottenheim, J., Niki, H., Langford, C. H. and Templeton, E. M. J.:

591   Photochemical bromine production implicated in Arctic boundary-layer ozone depletion, Nature, 355(6356), 150–

592   152, doi:10.1038/355150a0, 1992.

593   Neuman, J. A., Nowak, J. B., Huey, L. G., Burkholder, J. B., Dibb, J. E., Holloway, J. S., Liao, J., Peischl, J., Roberts,

594   J. M., Ryerson, T. B., Scheuer, E., Stark, H., Stickel, R. E., Tanner, D. J. and Weinheimer, A.: Bromine measurements

595   in ozone depleted air over the Arctic Ocean, Atmos Chem Phys, 10(14), 6503–6514, doi:10.5194/acp-10-6503-2010,

596   2010.

597   O'Driscoll, P., Lang, K., Minogue, N. and Sodeau, J.: Freezing Halide Ion Solutions and the Release of Interhalogens

598   to the Atmosphere, J. Phys. Chem. A, 110(14), 4615–4618, doi:10.1021/jp060491v, 2006.

599   O'Driscoll, P., Minogue, N., Takenaka, N. and Sodeau, J.: Release of Nitric Oxide and Iodine to the Atmosphere from

600   the Freezing of Sea-Salt Aerosol Components, J. Phys. Chem. A, 112(8), 1677–1682, doi:10.1021/jp710464c, 2008.

601   Oldridge, N. W. and Abbatt, J. P. D.: Formation of Gas-Phase Bromine from Interaction of Ozone with Frozen and

602   Liquid NaCl/NaBr Solutions: Quantitative Separation of Surficial Chemistry from Bulk-Phase Reaction, J. Phys.

603   Chem. A, 115(12), 2590–2598, doi:10.1021/jp200074u, 2011.

604 Orlando, F., Waldner, A., Bartels-Rausch, T., Birrer, M., Kato, S., Lee, M.-T., Proff, C., Huthwelker, T., Kleibert, A.,

605 Bokhoven, J. van and Ammann, M.: The Environmental Photochemistry of Oxide Surfaces and the Nature of Frozen

606 Salt Solutions: A New in Situ XPS Approach, Top. Catal., 1–14, doi:10.1007/s11244-015-0515-5, 2016.

607 O'Sullivan, D. and Sodeau, J. R.: Freeze-Induced Reactions: Formation of Iodine−Bromine Interhalogen Species from

608 Aqueous Halide Ion Solutions, J. Phys. Chem. A, 114(46), 12208–12215, doi:10.1021/jp104910p, 2010.

609 Oum, K. W., Lakin, M. J. and Finlayson-Pitts, B. J.: Bromine activation in the troposphere by the dark reaction of O_3

610 with seawater ice, Geophys. Res. Lett., 25(21), 3923–3926, doi:10.1029/1998GL900078, 1998a.

611 Oum, K. W., Lakin, M. J., DeHaan, D. O., Brauers, T. and Finlayson-Pitts, B. J.: Formation of Molecular Chlorine

612 from the Photolysis of Ozone and Aqueous Sea-Salt Particles, Science, 279(5347), 74–76,

613 doi:10.1126/science.279.5347.74, 1998b.

614 Platt, U. and Hönninger, G.: The role of halogen species in the troposphere, Chemosphere, 52(2), 325–338,

615 doi:10.1016/S0045-6535(03)00216-9, 2003.

616 Pratt, K. A., Custard, K. D., Shepson, P. B., Douglas, T. A., Pöhler, D., General, S., Zielcke, J., Simpson, W. R., Platt,

617 U., Tanner, D. J., Gregory Huey, L., Carlsen, M. and Stirm, B. H.: Photochemical production of molecular bromine

618 in Arctic surface snowpacks, Nat. Geosci., 6(5), 351–356, doi:10.1038/ngeo1779, 2013.

619 Raso, A. R. W., Custard, K. D., May, N. W., Tanner, D., Newburn, M. K., Walker, L., Moore, R. J., Huey, L. G.,

620 Alexander, L., Shepson, P. B. and Pratt, K. A.: Active molecular iodine photochemistry in the Arctic, Proc. Natl.

621 Acad. Sci., 114(38), 10053–10058, doi:10.1073/pnas.1702803114, 2017.

622 Saiz-Lopez, A. and von Glasow, R.: Reactive halogen chemistry in the troposphere, Chem. Soc. Rev., 41(19), 6448–

623 6472, doi:10.1039/C2CS35208G, 2012.

624 Shaw, M. D. and Carpenter, L. J.: Modification of Ozone Deposition and I $_2$ Emissions at the Air–Aqueous Interface

625 by Dissolved Organic Carbon of Marine Origin, Environ. Sci. Technol., 47(19), 10947–10954,

626 doi:10.1021/es4011459, 2013.

627 Simpson, W. R., von Glasow, R., Riedel, K., Anderson, P., Ariya, P., Bottenheim, J., Burrows, J., Carpenter, L. J.,

628 Frieß, U., Goodsite, M. E., Heard, D., Hutterli, M., Jacobi, H.-W., Kaleschke, L., Neff, B., Plane, J., Platt, U., Richter,

629 A., Roscoe, H., Sander, R., Shepson, P., Sodeau, J., Steffen, A., Wagner, T. and Wolff, E.: Halogens and their role in

630 polar boundary-layer ozone depletion, Atmos Chem Phys, 7(16), 4375–4418, doi:10.5194/acp-7-4375-2007, 2007.

631 Simpson, W. R., Brown, S. S., Saiz-Lopez, A., Thornton, J. A. and Glasow, R. von: Tropospheric Halogen Chemistry:

632 Sources, Cycling, and Impacts, Chem. Rev., 115(10), 4035–4062, doi:10.1021/cr5006638, 2015.

633 Sjostedt, S. J. and Abbatt, J. P. D.: Release of gas-phase halogens from sodium halide substrates: heterogeneous

634 oxidation of frozen solutions and desiccated salts by hydroxyl radicals, Environ. Res. Lett., 3(4), 045007,

635 doi:10.1088/1748-9326/3/4/045007, 2008.

636 Steffen, A., Douglas, T., Amyot, M., Ariya, P., Aspmo, K., Berg, T., Bottenheim, J., Brooks, S., Cobbett, F., Dastoor,

637 A., Dommergue, A., Ebinghaus, R., Ferrari, C., Gardfeldt, K., Goodsite, M. E., Lean, D., Poulain, A. J., Scherz, C.,

638 Skov, H., Sommar, J. and Temme, C.: A synthesis of atmospheric mercury depletion event chemistry in the

639 atmosphere and snow, Atmospheric Chem. Phys., 8(6), 1445–1482, doi:10.5194/acp-8-1445-2008, 2008.

640 Steffen, A., Bottenheim, J., Cole, A., Ebinghaus, R., Lawson, G. and Leaitch, W. R.: Atmospheric mercury speciation

641 and mercury in snow over time at Alert, Canada, Atmos Chem Phys, 14(5), 2219–2231, doi:10.5194/acp-14-2219-

642 2014, 2014.

643 Tang, T. and McConnell, J. C.: Autocatalytic release of bromine from Arctic snow pack during polar sunrise, Geophys.

644 Res. Lett., 23(19), 2633–2636, doi:10.1029/96GL02572, 1996.

645 Tsunogai, S. and Sase, T.: Formation of iodide-iodine in the ocean, Deep Sea Res. Oceanogr. Abstr., 16(5), 489–496,

646 doi:10.1016/0011-7471(69)90037-0, 1969.

647 Vogt, R., Crutzen, P. J. and Sander, R.: A mechanism for halogen release from sea-salt aerosol in the remote marine

648 boundary layer, Nature, 383(6598), 327–330, doi:10.1038/383327a0, 1996.

649 Wang, S. and Pratt, K. A.: Molecular Halogens above the Arctic Snowpack: Emissions, Diurnal Variations, and

650 Recycling Mechanisms, J. Geophys. Res. Atmospheres, 2017.

651 Weaver, J. R.: Birck Nanotechnology Center Technical Overview, edited by Purdue University Office of Research

652 and Partnerships, [online] Available from: http://docs.lib.purdue.edu/gendes/5 (Accessed 28 January 2016), 2015.

653 Wennberg, P.: Atmospheric chemistry: Bromine explosion, Nature, 397(6717), 299–301, doi:10.1038/16805, 1999.

654 Wren, S. N. and Donaldson, D. J.: How does deposition of gas phase species affect pH at frozen salty interfaces?,

655 Atmospheric Chem. Phys., 12(21), 10065–10073, doi:https://doi.org/10.5194/acp-12-10065-2012, 2012a.

656 Wren, S. N. and Donaldson, D. J.: Laboratory Study of pH at the Air–Ice Interface, J. Phys. Chem. C, 116(18), 10171–

657 10180, doi:10.1021/jp3021936, 2012b.

658   Wren, S. N., Donaldson, D. J. and Abbatt, J. P. D.: Photochemical chlorine and bromine activation from artificial

659   saline snow, Atmos Chem Phys, 13(19), 9789–9800, doi:10.5194/acp-13-9789-2013, 2013.

660   Xiong, F., McAvey, K. M., Pratt, K. A., Groff, C. J., Hostetler, M. A., Lipton, M. A., Starn, T. K., Seeley, J. V.,

661   Bertman, S. B., Teng, A. P., Crounse, J. D., Nguyen, T. B., Wennberg, P. O., Misztal, P. K., Goldstein, A. H.,

662   Guenther, A. B., Koss, A. R., Olson, K. F., de Gouw, J. A., Baumann, K., Edgerton, E. S., Feiner, P. A., Zhang, L.,

663   Miller, D. O., Brune, W. H. and Shepson, P. B.: Observation of isoprene hydroxynitrates in the southeastern United

664   States and implications for the fate of NOx, Atmos Chem Phys, 15(19), 11257–11272, doi:10.5194/acp-15-11257-

665   2015, 2015.

666   Zehavi, D. and Rabani, J.: Oxidation of aqueous bromide ions by hydroxyl radicals. Pulse radiolytic investigation, J.

667   Phys. Chem., 76(3), 312–319, doi:10.1021/j100647a006, 1972.

668

669 **Tables**

670 Table 1: List of relevant species monitored by chemical ionization mass spectrometry ($I(H_2O)_n^-$ as reagent ion) with corresponding
671 *m/z* values.

Species	*m/z*
$I^{81}Br^-$	208
$I^{79}Br^{79}Br^-$	285
$I^{79}Br^{81}Br^-$	287
$I^{35}Cl^-$	162
$I^{37}Cl^-$	164
$I^{35}Cl^{35}Cl^-$	197
$I^{35}Cl^{37}Cl^-$	199
$I^{37}Cl^{37}Cl^-$	201
$I^{79}Br^{35}Cl^-$	241
$I^{81}Br^{35}Cl^-$ / $I^{79}Br^{37}Cl^-$	243
I_3^-	381
$IHO^{79}Br$	223
$IHO^{81}Br$	225
$IHO_3^5Cl^-$	179
$IHO_3^7Cl^-$	181
$IHOI^-$	271
$I^{79}IBr^-$	333
$I^{81}IBr^-$	335

672

673

674 Table 2: Results for all experiments performed. The first line in an experiment represents the integrated totals of molecular halogen
675 production after 1 hour of irradiation (t = 0 through t =1 h). The results on italicized lines are 1 h integrated production amounts
676 beginning once additional ozone was introduced to the flow tube. Average LODs across experiments were 1.8 ± 0.4, 1.2 ± 0.3,
677 and 9 ± 2 pmol mol^{-1} for Br$_2$, Cl$_2$, and I$_2$ respectively. "IO#" represents samples composed of Instant Ocean, and "SW#" represents
678 "saltwater" samples, composed of reagent salts. "CL1" here represents the experiment performed using 0.557M high purity NaCl.
679 *The Br$_2$ and I$_2$ values presented for IO2 are discussed further in the Supplemental Information.

Experiment	Oxidant	pH	I$_2$ produced (nmol)	Br$_2$ produced (nmol)	Cl$_2$ produced (nmol)
IO1	H$_2$O$_2$	4.7	9 (±3)	< LOD	
	+O$_3$		*22 (±8)*	*0.06 (±0.05)*	
IO2	H$_2$O$_2$	4.7	*0.6 (±0.4)	*0.034 (±0.003)	
	+O$_3$		*21 (±14)*	*0.038 (±0.003)*	
SW1	H$_2$O$_2$	4.7	6.0 (±2.1)	< LOD	
	+O$_3$		*51 (±19)*	*0.024(±0.014)*	
SW2	H$_2$O$_2$	4.5	8 (±4)	< LOD	
	+O$_3$		*51 (±25)*	*0.018 (±0.003)*	
IO3	NO$_2^-$	2.0	39 (±1)	0.084 (±0.002)	
IO4	H$_2$O$_2$	1.7	0.8 (±0.3)	5.6 (±0.3)	
	+O$_3$		*< LOD*	*12 (±1)*	
IO5	H$_2$O$_2$	1.7	0.33 (±0.11)	3.5 (±0.4)	
	+O$_3$		*0.11 (±0.04)*	*9.2 (±1.0)*	
SW3	NO$_2^-$	1.8	4.0 (±0.1)	< LOD	
	+O$_3$		*< LOD*	*0.46 (±0.1)*	
SW4	NO$_2^-$	2.2	< LOD	5.4 (±0.7)	
	+O$_3$		*< LOD*	*13 (±2)*	
SW5	H$_2$O$_2$	1.8	0.75 (±0.26)	6.0 (±0.7)	
	+O$_3$		*< LOD*	*15 (±2)*	
CL1	H$_2$O$_2$	1.8	0.10 (±0.03)	0.10 (±0.01)	0.093 (±0.008)
IO6	None	4.7	< LOD	< LOD	
	+O$_3$		*26 (±9)*	*0.015 (±0.001)*	
IO7	None	4.7	0.10 (±0.06)	< LOD	
	+O$_3$		*47 (±29)*	*0.012 (±0.001)*	
SW6	None	4.7	< LOD	< LOD	
	+O$_3$		*80 (±1)*	*0.16 (±0.01)*	
SW7	None	4.5	< LOD	< LOD	
	+O$_3$		*48 (±2)*	*0.023 (±0.001)*	
IO8	None	2.0	14 (±10)	< LOD	
	+O$_3$		*2.6 (±1.7)*	*0.14 (±0.02)*	
SW8	None	2.0	14 (±10)	< LOD	
	+O$_3$		*2.6 (±1.7)*	*0.14 (±0.02)*	

680

681 **Figures**

682

683 Figure 1: Experimental schematic. Purple bars represent powered solar simulator bulbs. The green shading around the flow tube
684 (flow reactor) represents cooling liquid (60% ethylene glycol, 40% water) circulated through the chiller. The flow reactor region
685 itself has an inner diameter of 2.5 cm.

686

687
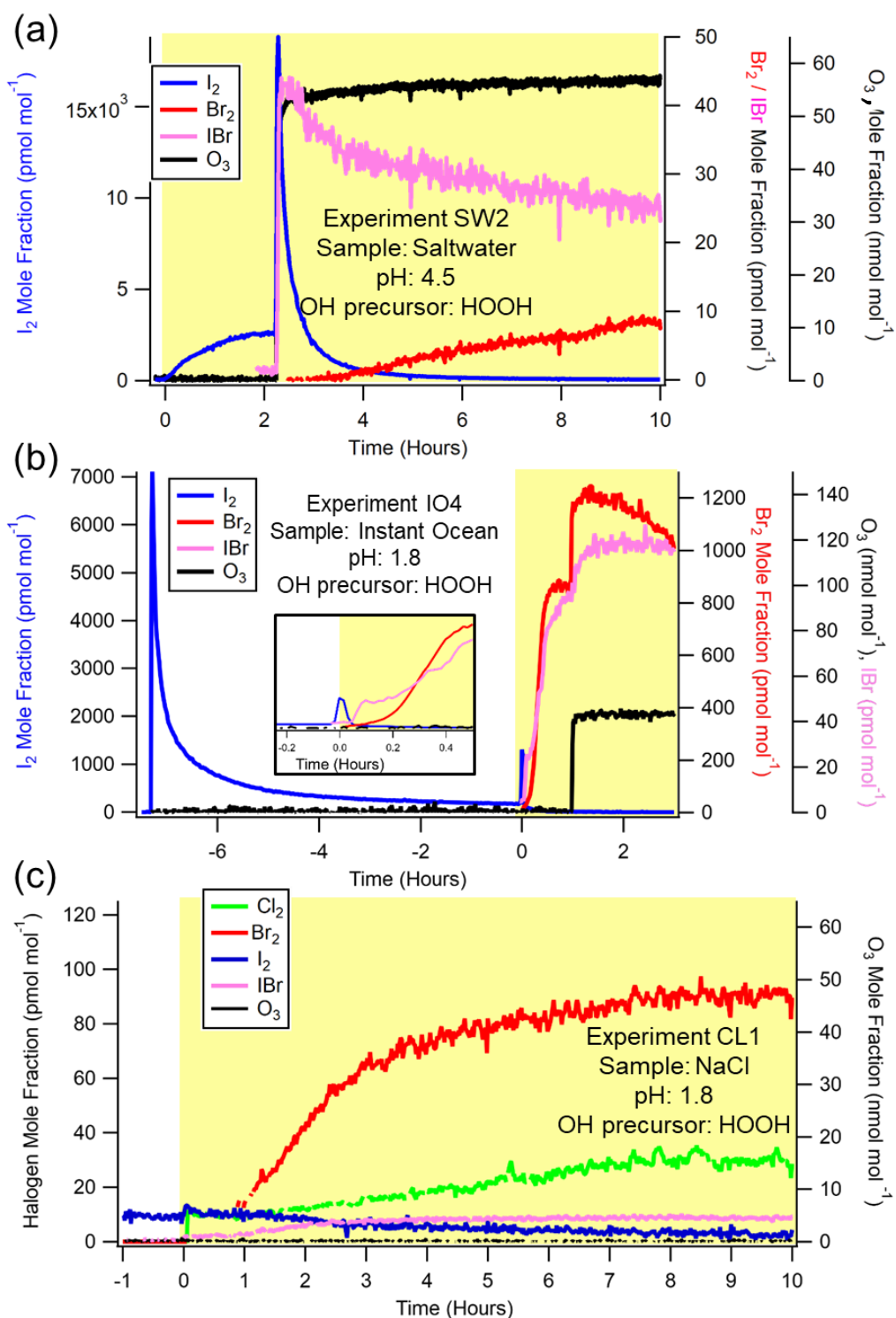
Figure 2: Representative experiments of OH-mediated production of X_2, and subsequent production of X_2 from O_3 addition. a)
Saltwater experiment (SW2) at pH=4.5. b) Instant Ocean experiment (IO4) at pH = 1.8. Time varying Br_2 and IBr signals before
t=0 are shown in Fig. S2. Inset more clearly shows the increase of I_2 signal after irradiation. c) NaCl experiment (CL1) at pH = 1.8.
Timescale represents hours from the activation of the lights, and the yellow shading represents presence of radiation from solar
simulator bulbs. Gaps in data represent periods when the isotopic ratios showed an interference.

693
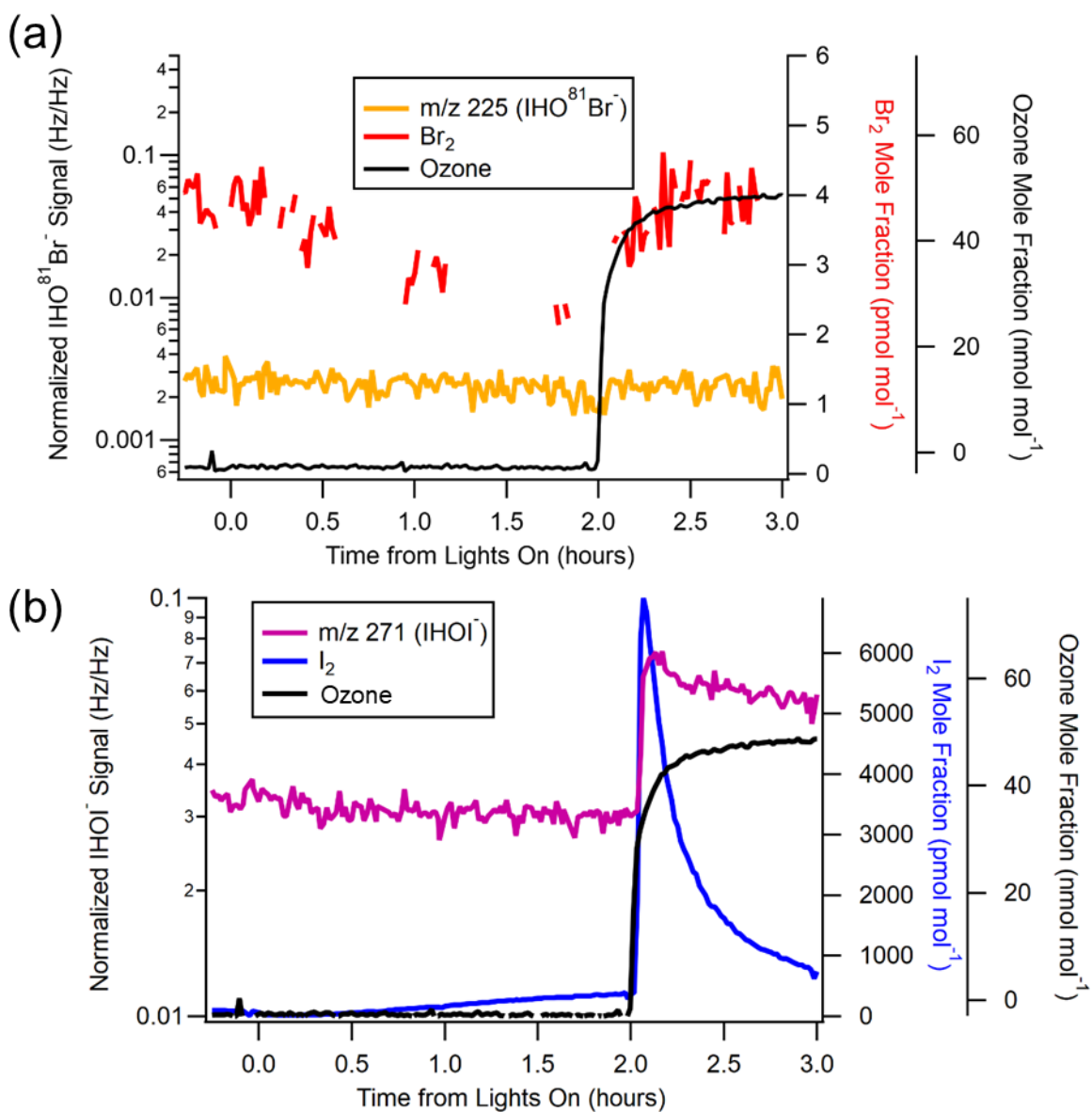
Figure 3: Normalized, background subtracted HOX signals from experiment IO2, pH=4.7. a) Comparison of Br_2 mole fractions to
695   HOBr (*m/z* 225). Note that the HOBr signal should be considered only qualitatively as its identity could not be confirmed using
696   isotopic ratios with *m/z* 223 due to its relatively large background signal. b) Effect of O_3 on I_2 and HOI.

697
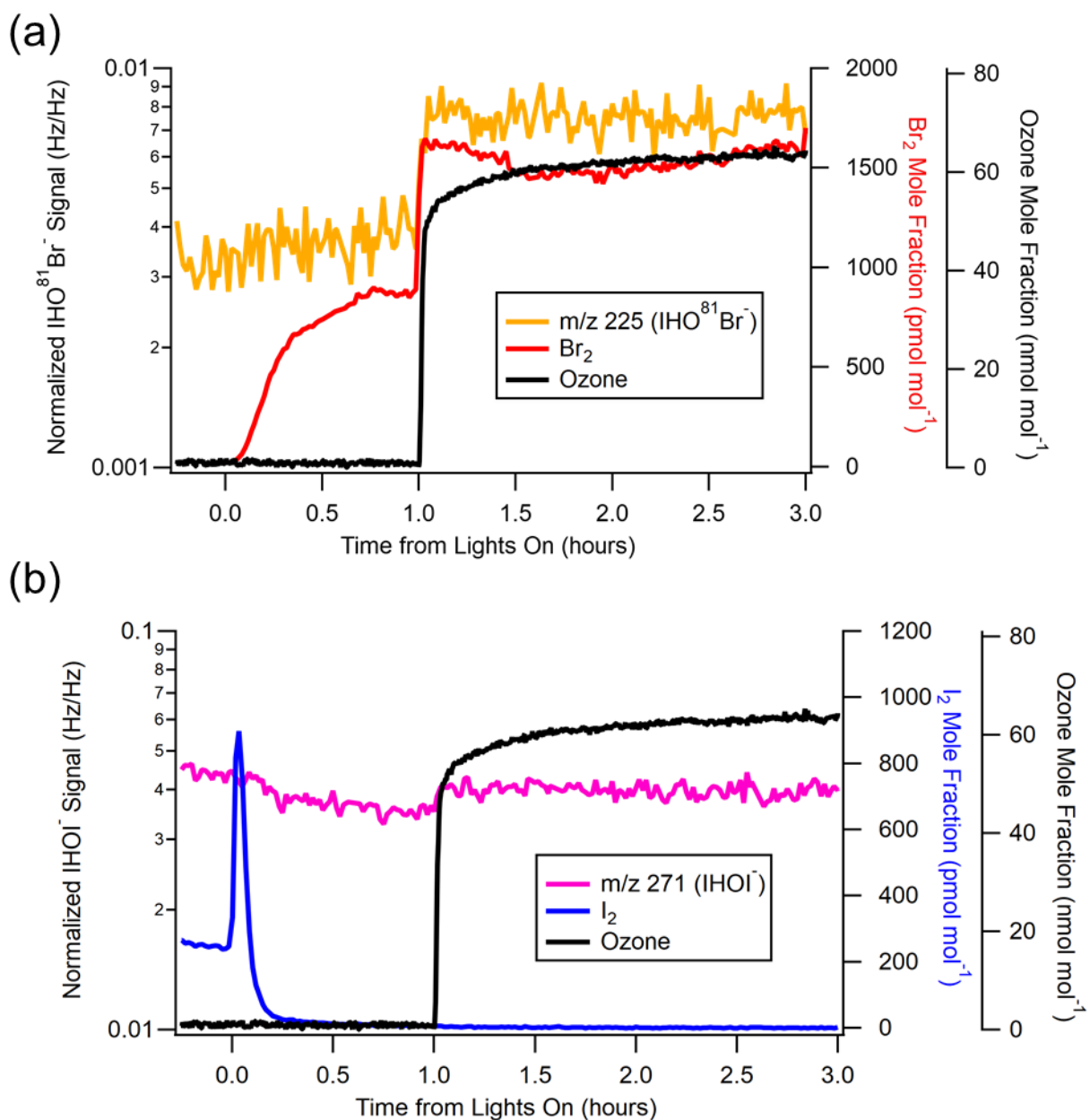
698

699 Figure 4: Normalized, background subtracted HOX signals from experiment SW5, pH=1.8. a) Comparison of Br_2 mole fractions
700 to HOBr (*m/z* 225). Note that the HOBr signal should be considered only qualitatively as its identity could not be confirmed using
701 isotopic ratios with *m/z* 223. b) Effect of O_3 on I_2 and HOI.

702